

Article

Preparation, Characterization, and In Vitro Evaluation of the Biological Activity of Several Metal-Based Complexes with Two Widely Used Fluoroquinolone Antibiotics: Lomefloxacin and Pefloxacin Drugs

Abdulrahman A. Almehezia ¹, Mohamed A. Al-Omar ¹, Ahmed M. Naglah ^{1,*}, Mashooq A. Bhat ², Razan Eskandrani ², Fatimah A. Alotaibi ³, Moamen S. Refat ⁴ and Abdel Majid A. Adam ⁴

¹ Drug Exploration and Development Chair (DEDC), Department of Pharmaceutical Chemistry, College of Pharmacy, King Saud University, P.O. Box 2457, Riyadh 11451, Saudi Arabia; mehizia@ksu.edu.sa (A.A.A.); malomar1@ksu.edu.sa (M.A.A.-O.)

² Department of Pharmaceutical Chemistry, College of Pharmacy, King Saud University, P.O. Box 2457, Riyadh 11451, Saudi Arabia; mabhat@ksu.edu.sa (M.A.B.); razan.a.esk@gmail.com (R.E.)

³ Department of Chemistry, Faculty of Science, University of Tabuk, P.O. Box 741, Tabuk 71491, Saudi Arabia; f-alotaibi@ut.edu.sa

⁴ Department of Chemistry, College of Science, Taif University, P.O. Box 11099, Taif 21944, Saudi Arabia; moamen@tu.edu.sa (M.S.R.); majidadam@tu.edu.sa (A.M.A.A.)

* Correspondence: anaglah@ksu.edu.sa

Abstract: Lomefloxacin (F1) and pefloxacin (F2) have a broad spectrum of antimicrobial activities against gram-positive and gram-negative bacteria. In this study, we investigated the complexation mode, morphological, and biological properties of four metal-based complexes of F1 and F2 molecules with Mg(II), Ca(II), Zn(II), and Fe(III) metal ions. These complexes were prepared at ~60–70 °C in a neutral medium using a 5% NH₃ solution at pH ~7–8 with a 1:1 ratio. Multiple physicochemical methods were employed to characterize the binding mode between F1 and F2 with the metal ions under investigation. The results of these methods suggested that the gross formula of the complexes obtained with the metal ions were [mgf1(H₂O)Cl]·2H₂O, [caf1(H₂O)Cl]·3H₂O, [znf1(H₂O)Cl], [fef1(H₂O)₂Cl₂]·Cl·2H₂O, [mgf2(H₂O)Cl]·2H₂O, [caf2(H₂O)Cl]·3H₂O, [znf2(H₂O)Cl], and [fef2(H₂O)₂Cl₂]·Cl·2H₂O. The microscopic characterizations indicated that the Ca(II)-F1 complex had an interesting surface topography. Its particles had a homogenous, short, rod-like shaped structure that clustered together to form a tree shape. Using the Kirby–Bauer disc diffusion protocol, the synthesized metal-based complexes were screened in vitro against different gram-positive and gram-negative bacterial and fungal species. The antimicrobial profile of the Fe(III)-F1 complex indicated that it had remarkable inhibitory activity against all the tested bacterial and fungal species with a potency equal to that of the standard drugs (streptomycin and ketoconazole).

Keywords: fluoroquinolones; lomefloxacin; pefloxacin metal-based complex; spectroscopies; biological activities



Citation: Almehezia, A.A.; Al-Omar, M.A.; Naglah, A.M.; Bhat, M.A.; Eskandrani, R.; Alotaibi, F.A.; Refat, M.S.; Adam, A.M.A. Preparation, Characterization, and In Vitro Evaluation of the Biological Activity of Several Metal-Based Complexes with Two Widely Used Fluoroquinolone Antibiotics: Lomefloxacin and Pefloxacin Drugs. *Crystals* **2023**, *13*, 1078. <https://doi.org/10.3390/cryst13071078>

Academic Editor: Marian Valko

Received: 18 June 2023

Revised: 3 July 2023

Accepted: 7 July 2023

Published: 10 July 2023



Copyright: © 2023 by the authors. Licensee MDPI, Basel, Switzerland. This article is an open access article distributed under the terms and conditions of the Creative Commons Attribution (CC BY) license (<https://creativecommons.org/licenses/by/4.0/>).

1. Introduction

Considerable interest has been focused on the coordination chemistry of metal-based complexes and metallodrugs by chemistry, biology, and pharmacology researchers. Metallodrugs are compounds that contain a drug molecule and a metal ion, and numerous metallodrugs possess potential pharmaceutical properties, such as antibacterial, anticancer, and antiviral properties. Metallodrugs are useful as chemotherapeutics and therapeutic agents for treating various human diseases, including cancer, diabetes, neurological disorders, and infections [1–8]. Polymers are widely used as biomaterials and have motivated

the development of biomedical fields because of their biocompatibility and biodegradability. Biodegradable and biocompatible polymers can be degraded or dissolved into the surrounding environment with no pollution. These polymers are promising for effectively relieving the environmental burden. Biodegradable polymers are usually biocompatible, which enables electronics to be used in implantable biomedical applications, such as medical devices. These polymeric biomaterials have emerged during the past decades to promise extraordinary breakthroughs in a wide range of diagnostic and therapeutic medical devices, including temporary implants and three-dimensional scaffolds for tissue engineering, as well as pharmacological applications, such as delivery vehicles for controlled/sustained drug release. Biopolymers are also used in the food packaging industry and agricultural and industrial processes [9–11].

Fluoroquinolones (fqs) are a class of compounds with strong and broad-spectrum antibacterial properties. Due to their low cost, high potency, and lack of cross-resistance, fqs have been widely used as antibiotics for over 30 years [12,13]. The complexation of fqs with different non-transition and transition metal ions has been extensively investigated to synthesize new metal-based complexes containing fqs, aiming to improve the pharmaceutical and biological characteristics of FQ antibiotics [14,15].

Two examples of the second-generation FQ antibiotic are lomefloxacin (F1) and pefloxacin (F2), which possess strong antibacterial, anti-inflammatory, and antifungal activities. Their structures are shown in Figure 1. The antibacterial activity spectrum of F1 and F2 includes gram-positive and -negative bacteria. F1 is commonly used to treat and prevent bacterial infections, urinary tract infections, and bronchitis, whereas F2 is used to treat gram-negative-bacterial infections in the genitourinary tract and gastrointestinal system and treat gonococcal urethritis. The literature includes several examples of metal-based complexes of F1 and F2 containing several metal ions such as Zn(II), Cu(II), Ni(II), Co(II), Pt(II), Cr(III), Fe(III), Bi(IV), and UO₂(II) [16–19]; some of these examples are listed in Table 1. We believe metal-based complexes can be utilized to design and develop more biologically active drugs. Therefore, we aim to explore new insights into drugs F1 and F2 to form new metal-based complexes and examine the synthesized complexes' pharmacological properties.

Table 1. Examples of F1 and F2 metal-based complexes.

Drug	Molar Ratio (Metal to Ligand)	Complexes	References
F1	1:1	[UO ₂ F1(H ₂ O) ₂](NO ₃) ₂	[16–18]
		[thf1(H ₂ O) ₄]Cl ₄	
		[znf1(H ₂ O) ₄]Cl ₂	
		[cuf1(H ₂ O) ₄]Cl ₂ ·2H ₂ O	
		[nif1(H ₂ O) ₄]Cl ₂ ·H ₂ O	
		[cof1(H ₂ O) ₄]Cl ₂	
F1	1:2	[fef1(H ₂ O) ₄]Cl ₃ ·H ₂ O	[16–18]
		[mnf1(H ₂ O) ₄]Cl ₂	
		[crf1(H ₂ O) ₄]Cl ₃	
F1	1:3	[zro(F1) ₂ Cl]Cl·15H ₂ O	[16–18]
		[Y(F1) ₂ Cl ₂]Cl·12H ₂ O	
		[UO ₂ (F1) ₃](NO ₃) ₂ ·4H ₂ O	
F2	1:1	[Bi(F1) ₃ (H ₂ O) ₂]	[16,19]
		-	
		[Pt(F2) ₂]	
F2	1:2	[Zn(F2) ₂ (H ₂ O)]·2H ₂ O	[16,19]
		[Bi(F2) ₃ (H ₂ O) ₂]	

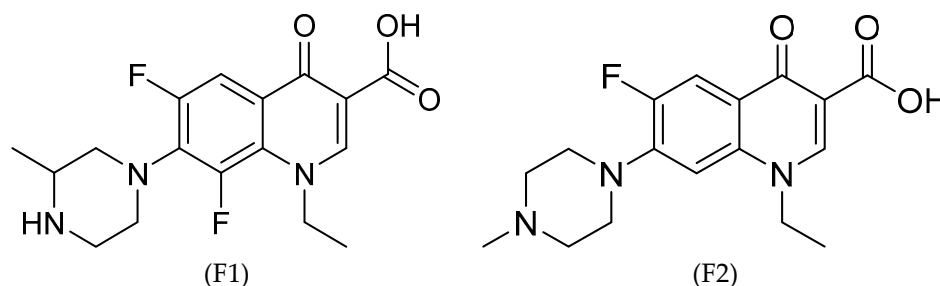


Figure 1. Structures of lomefloxacin (F1) and pefloxacin (F2).

This study focused on several parameters:

- (1) Synthesizing four metal-based complexes of F1 and F2 with Mg(II), Ca(II), Zn(II), and Fe(III) ions. The parameters of preparation were as follows: solvent—H₂O:meoh (1:1), reaction temperature—60–70 °C, media—neutral (ph 7–8), and molar ratio—1:1 (ligand to ion).
- (2) Employing several physicochemical approaches, including CHN elemental analyzer, ultraviolet/visible (UV-visible), Fourier-transform infrared (FT-IR), and nuclear magnetic resonance (¹H NMR) spectroscopies, to explore the complexation mode of F1 and F2 toward the metal ions under investigation.
- (3) Observing the surface morphology, phase purity, shapes, and sizes of the synthesized complexes' particles using scanning and transmission electron microscopy (SEM and TEM, respectively) and X-ray powder diffractometry (XRD).
- (4) Screening the synthesized metal-based complexes in vitro for their antimicrobial properties using the Kirby–Bauer disc diffusion assay method. The investigated microbes were *Bacillus subtilis*, *Streptococcus pneumoniae*, *Staphylococcus aureus*, *Escherichia coli*, and *Pseudomonas aeruginosa*, as well as three fungal microbes (*Aspergillus niger*, *Penicillium sp.*, and *Candida albicans*).

2. Materials and Methods

2.1. Materials

The analytical grade metal ion salts were obtained from Sigma-Aldrich (St. Louis, MO, USA), whereas F1 and F2 were obtained from Merck KGaA (Darmstadt, Germany). The metal ions and the ligands under investigation were:

- (i) Mg(II): MgCl₂ (95.21 g/mol; purity ≥ 98%);
- (ii) Ca(II): CaCl₂ (110.98 g/mol; purity 99.99%);
- (iii) Zn(II): ZnCl₂ (136.30 g/mol; purity ≥ 99.99 %);
- (iv) Fe(III): FeCl₃·6H₂O (270.30 g/mol; purity ≥ 98%);
- (v) F1: Lomefloxacin as HCl salt (C₁₇H₁₉F₂N₃O₃·HCl; 387.81 g/mol; purity ≥ 98%);
- (vi) F2: Pefloxacin as mesylate salt (C₁₇H₂₀FN₃O₃·CH₄O₃S·2H₂O; 465.49 g/mol; purity ≥ 98%).

2.2. Synthetic Methods

The Mg(II), Ca(II), Zn(II), and Fe(III) ions were complexed with F1 and F2 under the following conditions: solvent: H₂O:MeOH (1:1); reaction temperature: 60–70 °C; pH: neutral (7–8); and molar ratio: 1:1 (ligand to ion). The complexation process was as follows. First, four 100-mL beakers containing 20 mL of an aqueous solution of 2 mmol of MgCl₂, CaCl₂, ZnCl₂, and FeCl₃·6H₂O were prepared. Next, 20 mL of F1 solution (2 mmol) dissolved in MeOH was gradually added to each beaker. The mixtures were stirred with a magnetic stirrer at 60–70 °C. The pH of the mixtures was adjusted to ~7–8 using 5% ammonium solution, at which point colored precipitate began to form in each beaker. The four beakers were left on the hot plate for 10 min under continuous stirring and left overnight to ensure complete precipitation. Mg(II), Zn(II), and Fe(III) ions formed yellow-white colored precipitates, whereas Ca(II) ions formed yellow-colored precipitates. The resulting colored precipitates were filtered, washed with MeOH and CH₃CH₂OCH₂CH₃,

and subsequently dried in a vacuum desiccator over anhydrous CaCl_2 for 48 h. The Mg(II), Ca(II), Zn(II), and Fe(III) complexes of F2 were synthesized using the same procedure and were obtained as orange-yellow-colored powders for Mg(II) and Ca(II) ions, a white-colored powder for Zn(II) ions, and a brown-colored powder for Fe(III) ions. The eight synthesized metal-based complexes were subjected to elemental and spectral analyses, including UV-visible and FT-IR spectroscopy.

2.3. Characterization Methods

A Perkin-Elmer 2400 series CHN elemental analyzer, a Bruker DRX-250 Digital FT-NMR spectrometer, a Shimadzu FT-IR spectrophotometer, and a Perkin-Elmer Lambda 25 UV/Vis spectrophotometer were used to investigate the complexation mode of F1 and F2 with the metal ions. Elemental analysis data and spectra of ^1H NMR (600 MHz; $\text{DMSO-}d_6$), FT-IR (400–4000 cm^{-1}), and UV/Vis (200–1000 nm) were analyzed. Surface morphology, phase purity, and the size and shape of the synthesized complexes' particles were observed using a Quanta FEI 250 SEM, a JEOL JEM-1200 EX II TEM, and an X'Pert Philips X-ray diffractometer. SEM and TEM micrographs and the XRD patterns (2θ 5–90°) were used to analyze the synthesized complexes.

2.4. Antimicrobial Assays

The well-known Kirby–Bauer disc diffusion protocol [20–22] was used to evaluate the in vitro antimicrobial activities (antibacterial and antifungal) of the synthesized metal-based complexes. The complexes were prepared at a 100 $\mu\text{g}/\text{mL}$ concentration and screened against seven microbes isolated from clinical samples, including five bacterial species and three fungal species. The tested microbes were listed in Table 2.

Table 2. The tested microbes.

Microbe	Abbreviation
(A) Gram-positive bacterial strains	
<i>Bacillus subtilis</i>	<i>B. subtilis</i>
<i>Streptococcus pneumoniae</i>	<i>S. pneumoniae</i>
<i>Staphylococcus aureus</i>	<i>S. aureus</i>
(B) Gram-negative bacterial strains	
<i>Escherichia coli</i>	<i>E. coli</i>
<i>Pseudomonas aeruginosa</i>	<i>P. aeruginosa</i>
(C) Fungal strains	
<i>Aspergillus niger</i>	<i>A. niger</i>
<i>Penicillium</i> sp.	-
<i>Candida albicans</i>	<i>C. albicans</i>

The measured antibacterial susceptibility of the complexes was compared with standard antibiotic drugs (streptomycin for antibacterial assays and ketoconazole for antifungal assays).

3. Results and Discussion

3.1. Compositions and UV-Visible Spectra

Four metal-based complexes of F1 and four metal-based complexes of F2, with the metal ions Mg(II), Ca(II), Zn(II), and Fe(III), were synthesized directly from the reaction of F1 and F2 with the metal ions. The chloride salts of the metal ions were dissolved in H_2O , and F1 and F2 were dissolved in MeOH solvent. The reactions were carried out under specific conditions: (i) the solvent was $\text{H}_2\text{O}:\text{MeOH}$ (1:1), (ii) the reaction temperature was 60–70 °C, (iii) the media was neutral (pH 7–8), and (iv) the molar reaction was 1:1 (ligand

to ion). The complexes of F1 with Mg(II), Zn(II), and Fe(III) ions were yellow-white, and the complex with Ca(II) ions was completely yellow. The complexes of F2 with Mg(II) and Ca(II) ions were orange-yellow, the complex with Zn(II) ions was white, and the complex with Fe(III) ions was brown. Table 1 provides the microanalytical results of the synthesized metal-based complexes, including the contents in (%) of C, H, N, and Cl, which were determined by a CHN elemental analyzer, as well as the contents (%) of H₂O and metal, which were determined gravimetrically.

The data in Table 3 suggest that the general compositions of the F1 metal-based complexes obtained with Mg(II), Ca(II), Zn(II), and Fe(III) ions were [MgF1(H₂O)Cl]·2H₂O, [CaF1(H₂O)Cl]·3H₂O, [ZnF1(H₂O)Cl], and [FeF1(H₂O)₂Cl₂]·Cl·2H₂O, respectively. The corresponding gross formulas were C₁₇H₂₄F₂N₃O₆MgCl (464.12), C₁₇H₂₆F₂N₃O₇CaCl (497.89), C₁₇H₂₀F₂N₃O₄ZnCl (469.19), and C₁₇H₂₇F₂N₃O₇FeCl₃ (585.56 g/mol), respectively. The microanalytical results also suggest that the obtained complexes of F2 are formulated as [MgF2(H₂O)Cl]·2H₂O, [CaF2(H₂O)Cl]·3H₂O, [ZnF2(H₂O)Cl], and [FeF2(H₂O)₂Cl₂]·Cl·2H₂O, corresponding to gross formulas of C₁₇H₂₅FN₃O₆MgCl (446.12), C₁₇H₂₈FN₃O₇CaCl (479.89), C₁₇H₂₂FN₃O₄ZnCl (451.19), and C₁₇H₂₉FN₃O₇FeCl₃ (567.56 g/mol), respectively. The silver nitrate test confirmed that one Cl[−] ion was present outside of the coordination sphere for the [FeF1(H₂O)₂Cl₂]·Cl·2H₂O and [FeF2(H₂O)₂Cl₂]·Cl·2H₂O complexes.

Table 3. Microanalytical data of the F1 and F2 metal-based complexes with Mg(II), Ca(II), Zn(II), and Fe(III) ions.

Complex	Elemental Results (%)					
	Found (Calculated)					
	C	H	N	Cl	H ₂ O	Metal
Mg(II)-F1	44.06 (43.95)	5.35 (5.17)	8.93 (9.05)	7.50 (7.64)	11.45 (11.63)	5.46 (5.24)
Ca(II)-F1	40.73 (40.97)	5.10 (5.22)	8.59 (8.44)	7.30 (7.12)	14.62 (14.46)	7.94 (8.05)
Zn(II)-F1	43.60 (43.48)	4.18 (4.26)	9.10 (8.95)	7.43 (7.56)	4.00 (3.84)	13.70 (13.93)
Fe(III)-F1	34.96 (34.84)	4.31 (4.61)	7.30 (7.17)	17.94 (18.16)	12.09 (12.30)	9.43 (9.54)
Mg(II)-F2	45.60 (45.73)	5.76 (5.60)	9.57 (9.41)	7.80 (7.95)	12.32 (12.10)	5.70 (5.45)
Ca(II)-F2	42.39 (42.51)	5.99 (5.83)	8.86 (8.75)	7.56 (7.39)	14.77 (15.00)	8.26 (8.35)
Zn(II)-F2	45.35 (45.21)	4.79 (4.88)	9.45 (9.31)	7.70 (7.86)	3.92 (3.99)	14.62 (14.49)
Fe(III)-F2	35.70 (35.94)	5.00 (5.11)	7.22 (7.40)	18.95 (18.74)	12.85 (12.69)	9.97 (9.84)

The complexes of F1 and F2 with Mg(II) and Fe(III) ions were dissolved in a dimethylsulfoxide (DMSO) solution, and their UV-visible spectra were recorded in the 200–1000 nm wavelength range, as shown in Figure 2. The spectra of the four complexes displayed a strong, broad absorption band in the 260–500 nm range for Mg(II)-F1, 260–400 nm for Fe(III)-F1, 260–450 nm for Mg(II)-F2, and 260–600 nm for the Fe(III)-F2 complex. These absorption bands, with a maximum wavelength (λ_{\max}) at approximately ~320 nm, may be due to intra-ligand transitions ($n \rightarrow \pi^*$; $\pi \rightarrow \pi^*$). The UV-visible spectrum of the Fe(III)-F2 complex also exhibited a weak absorption band at 500 nm, which may be due to the metal-to-ligand charge transfer band (MLCT) [23,24]. The widening of the absorption bands decreased in a specific order: Mg(II)-F2 > Mg(II)-F1 > Fe(III)-F2 > Fe(III)-F1.

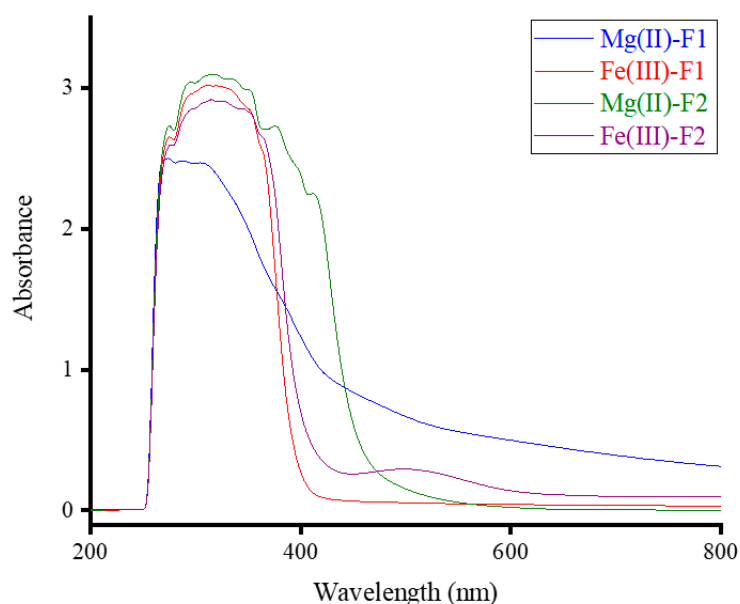


Figure 2. The UV-visible spectra of the F1 and F2 complexes with Mg(II) and Fe(III) ions.

3.2. FT-IR Spectra

3.2.1. Complexes of F1

Figure 3 contains the FT-IR spectra for free F1 and its metal-based complexes. The IR spectrum of free F1 molecule was characterized by:

- (i) A strong, broad absorption band with a single head appeared at 3438 cm^{-1} . This broadband could be assigned to the $\nu(\text{O-H})$ vibrations of the COOH group in the molecule and to moisture water.
- (ii) A medium-intensity absorption band resonated at 2938 cm^{-1} , and this band could be referred to as the $\nu(\text{N-H})_{\text{piperazine}}$ vibrations [25].
- (iii) A strong broad absorption band in the region from 2900 to 2600 cm^{-1} with multi-heads. These heads had different intensities and were located at 2892 , 2841 , 2760 , 2703 , and 2660 cm^{-1} . All these heads originated from $\nu_{\text{asym}}(\text{C-H})$ and $\nu_{\text{sym}}(\text{C-H})$ vibrations of CH, CH₃, and CH₂ moieties.
- (iv) A group of three very strong and sharp absorption bands resonated at 1724 , 1620 , and 1492 cm^{-1} . The band at 1492 cm^{-1} had a shoulder band with medium intensity located at 1529 cm^{-1} . The bands at 1719 and 1625 cm^{-1} were generated from the $\nu(\text{C=O})_{\text{COOH}}$ and $\nu(\text{C=O})_{\text{pyridone}}$ vibrations, respectively. The band at 1492 cm^{-1} was due to the $\delta_{\text{def}}(\text{CH}_2)$ vibrations, whereas its shoulder at 1529 cm^{-1} could be referred to as the $\nu(\text{C=C})$ vibrations [26].
- (v) A group of medium-intensity bands resonated at 1333 , 1257 , 1212 , 1096 , 1042 , and 807 cm^{-1} were generated from the vibrations of $\delta_{\text{sciss}}(\text{CH}_2)$, $\nu_{\text{asym}}(\text{C-N})$, $\nu(\text{C-O})$, $\nu(\text{C-F})$, $\nu_{\text{sym}}(\text{C-N})$, and $\delta_{\text{wag}}(\text{CH}_3)$, respectively [27].

In the FT-IR spectra of the F1 complexes with Mg(II), Ca(II), and Zn(II) ions, the absorption band due to the $\nu(\text{C=O})_{\text{COOH}}$, which appeared at 1724 cm^{-1} in the free F1 molecule, was absent, which suggests the formation of an ionic bond between Mg(II), Ca(II), and Zn(II) metal ions with the oxygen atom of the carboxylate group of the F1 molecule. The band originated from the $\nu(\text{C=O})_{\text{pyridone}}$ vibrations, which appeared at 1625 cm^{-1} in the FT-IR spectrum of the free F1 molecule, was shifted to lower frequencies in the FT-IR spectra of the Mg(II) (1610 cm^{-1}), Ca(II) (1609 cm^{-1}), and Zn(II) (1610 cm^{-1}) complexes. This proposed that the C=O group of the pyridone ring in the F1 molecule participated in the chelation process with these metal ions [28,29]. In the FT-IR spectrum of the F1 complex with Fe(III) ions, the bands due to the $\nu(\text{C=O})_{\text{COOH}}$ and $\nu(\text{C=O})_{\text{pyridone}}$ were slightly shifted to 1720 and 1623 cm^{-1} , respectively, suggesting that the carboxylic group ($-\text{COOH}$) and

C=O group of pyridone ring were not participating in the coordination process, and these groups were far away from the place of coordination in the F1 molecule with Fe(III) ions. The bands resulted from the $\nu(\text{N-H})_{\text{piperazine}}$, $\nu_{\text{asym}}(\text{C-N})$ and $\nu_{\text{sym}}(\text{C-N})$ vibrations were shifted from 2938, 1257, and 1096 cm^{-1} in the free F1 molecule to 2900, 1240, and 1052 cm^{-1} in the Fe(III) complex. New medium-intensity absorption bands appeared in the FT-IR spectra of Mg(II), Ca(II), Zn(II), and Fe(III) complexes at (498 and 458 cm^{-1}), (491 and 450 cm^{-1}), (500 and 460 cm^{-1}), and (503 and 485 cm^{-1}), respectively. These two bands could be assigned to the $\nu(\text{M-N})$ and $\nu(\text{M-O})$ vibrations, respectively [27]. All these IR spectral observations suggested that the F1 molecule was coordinated to the Mg(II), Ca(II), and Zn(II) ions via the oxygen atoms of the carboxylate group and the pyridone C=O group, whereas the F1 molecule was coordinated to the Fe(III) ions via the two nitrogen atoms of the piperazine ring.

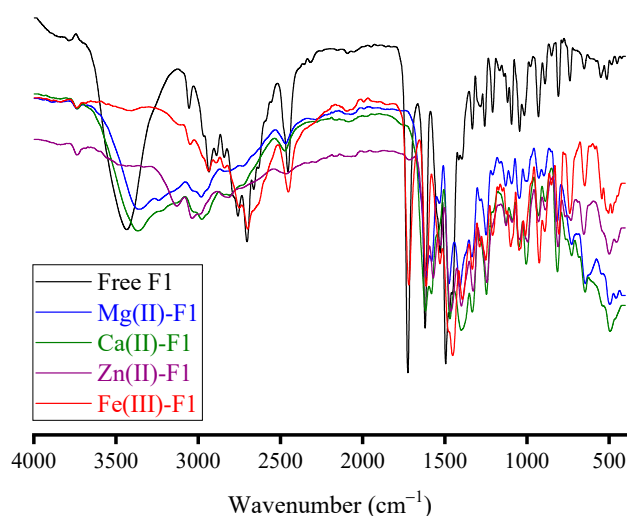


Figure 3. The FT-IR spectra of the free F1 and its metal-based complexes.

3.2.2. Complexes of F2

Figure 4 presents the FT-IR spectra for free F2 and its metal-based complexes. The IR spectrum of the free F2 molecule was characterized by:

- (i) A strong, broad absorption band with a single head appeared at 3450 cm^{-1} , originating from the vibrations of the O–H bond of –the COOH group in the molecule and moisture water.
- (ii) A medium-intensity broad absorption band with three heads appeared at 3055, 2985, and 2930 cm^{-1} . These heads were due to the $\nu_{\text{asym}}(\text{C-H})$ and $\nu_{\text{sym}}(\text{C-H})$ vibrations of CH, CH₃, and CH₂ moieties.
- (iii) A strong, broad absorption band in the region from 2700 to 2400 cm^{-1} with three heads. These heads had different intensities and resonated at 2647, 2578, and 2454 cm^{-1} . This broad band could be assigned to the $\nu(\text{NH}^+) - \text{CH}_3$ vibrations.
- (iv) A group of three strong and sharp absorption bands located at 1715, 1635, and 1486 cm^{-1} . The band at 1486 cm^{-1} had a medium-intensity shoulder band located at 1518 cm^{-1} . The absorptions at 1715, 1635, 1518, and 1486 cm^{-1} were due to the $\nu(\text{C=O})_{\text{COOH}}$, $\nu(\text{C=O})_{\text{pyridone}}$, $\nu(\text{C=C})$, and $\delta_{\text{def}}(\text{CH}_2)$ vibrations, respectively [26].
- (v) Absorptions at 1405, 1273, 1202, 1093, and 1053 cm^{-1} had different intensities and could be referred to as the vibrations of $\delta_{\text{sciss}}(\text{CH}_2)$, $\nu_{\text{asym}}(\text{C-N})$, $\nu(\text{C-O})$, $\nu(\text{C-F})$, and $\nu_{\text{sym}}(\text{C-N})$, respectively [27].

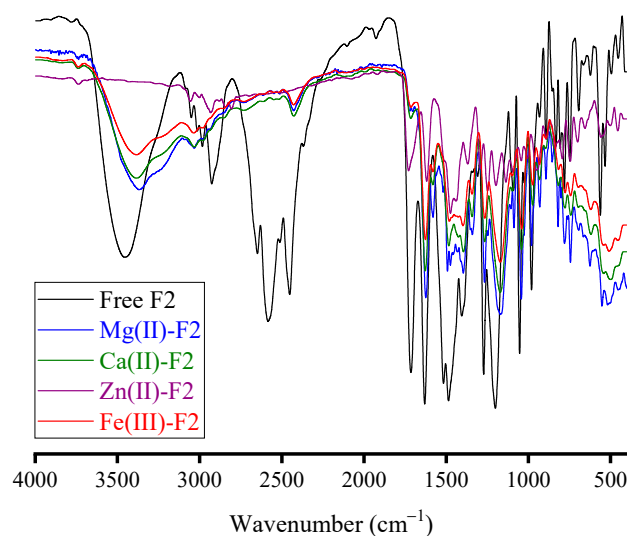


Figure 4. The FT-IR spectra of the free F2 and its metal-based complexes.

The absorption band originated from the $\nu(\text{C}=\text{O})_{\text{COOH}}$ vibration, which appeared at 1715 cm^{-1} in the FT-IR spectrum of the free F2 molecule, was no longer observed in the FT-IR spectra of the Mg(II), Ca(II), and Zn(II) complexes. The band due to the $\nu(\text{C}=\text{O})_{\text{pyridone}}$ was shifted from 1635 cm^{-1} in free F2 to around 1620 cm^{-1} in its complexes with Mg(II), Ca(II), and Zn(II) ions. This proposed that the F2 molecule captured these metal ions through the oxygen atom of the carboxylate group (ionic bond) and the oxygen atom of the pyridone C=O group (coordination bond) [28,29]. As observed in the Fe(III)-F1 complex, in the Fe(III)-F2 complex, the absorption bands originated from the $\nu(\text{C}=\text{O})_{\text{COOH}}$ and $\nu(\text{C}=\text{O})_{\text{pyridone}}$ vibrations slightly shifted. The bands that resulted from the $\nu_{\text{asym}}(\text{C}-\text{N})$ and $\nu_{\text{sym}}(\text{C}-\text{N})$ vibrations were shifted from 1273 and 1053 cm^{-1} in the free F2 molecule to 1252 and 1030 cm^{-1} in the Fe(III) complex, respectively. The $\nu(\text{M}-\text{N})$ and $\nu(\text{M}-\text{O})$ vibrations were responsible for the new absorption bands that appeared at $(508, 455\text{ cm}^{-1})$, $(500, 470\text{ cm}^{-1})$, $(495, 447\text{ cm}^{-1})$, and $(505, 455\text{ cm}^{-1})$ in the spectra of the Mg(II), Ca(II), Zn(II), and Fe(III) complexes, respectively. All these IR spectral observations suggested that the F2 molecule captured the Mg(II), Ca(II), and Zn(II) ions via the oxygen atoms of the carboxylate group and the pyridone C=O group, whereas the F2 molecule captured the Fe(III) ions via the two nitrogen atoms of the piperazine ring.

3.2.3. ^1H NMR Spectral Analysis

Figure 5 contains the ^1H NMR spectrum of the F1-Zn(II) complex collected in a $\text{DMSO}-d_6$ solvent at room temperature. The ^1H NMR chemical shifts obtained from the complex's spectrum are listed in Table 4 and compared with the free F1 molecule [30]. In the complex spectrum, the signals located at 2.27 and 2.28 ppm could be attributed to protons of $-\text{CH}_3$ moieties, and the protons of $-\text{CH}_2$ moieties could be responsible for the signals appearing at 6.57 and 6.59 ppm. The aromatic protons and the pyridine ring's protons resonated in the 7.44–7.46 ppm range. The characteristic signal due to the $(-\text{COOH})$ proton, which is observed at $\delta 11.78$ ppm in the spectrum of the free F1, is no longer observed in the spectrum of the complex. This suggested the deprotonation of the $-\text{COOH}$ group and the participation in complexation with Zn(II) ion. The signal that appeared at 3.36 ppm may be due to the protons of the coordinated water molecules.

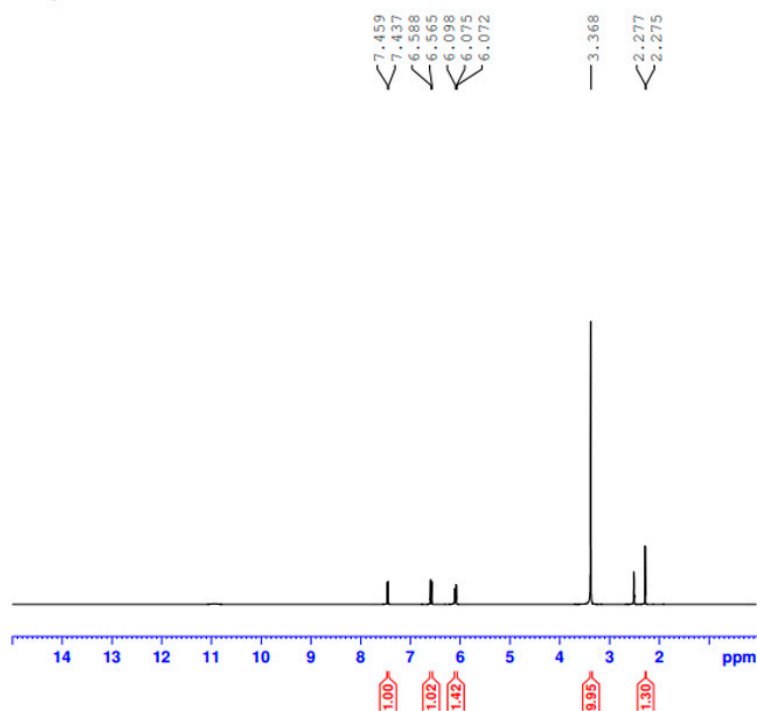


Figure 5. The ^1H NMR spectrum of the F1-Zn(II) complex.

Table 4. ^1H NMR data (ppm) of the free F1 molecule and its complex with the Zn(II) ion.

Free F1	F1-Zn(II)	Assignments
1.32–1.76	2.27, 2.28	δ 3H, $-\text{CH}_3$, $-\text{CH}_2\text{CH}_3$ δ 3H, $-\text{CH}_3$; attached to piperazine ring
3.55–4.21	6.07, 6.08, 6.98	δ 7H; piperazine ring protons
4.63–4.69	6.57, 6.59	δ 2H, $-\text{CH}_2$, $-\text{CH}_2\text{CH}_3$
7.79, 8.90	7.44, 7.46	δ H, $-\text{CH}$; benzene ring and pyridine ring
10.19–10.31	-	δ H, $-\text{NH}_2^+$; piperazine ring
11.78	-	δ H, $-\text{COOH}$

3.3. Proposed Structures

Structures of the F1 and F2 metal-based complexes with Mg(II), Ca(II), Zn(II), and Fe(III) ions were proposed based on the analytical (C, H, N, Cl, metal analysis) and spectral (UV–visible, IR, ^1H NMR) results and described in Figure 6. In these structures, F1 and F2 coordinate the Mg(II), Ca(II), and Zn(II) ions in a bidentate manner using the oxygen atoms of the carboxylate group and the pyridone C=O group, whereas F1 and F2 bind to the Fe(III) ion using the two nitrogen atoms of the piperazine ring. The coordination spheres around the metal ions are complemented by water molecules. The capturing of the metal ions under investigation by F1 and F2 result in complexes with the following proposed molecular formulas: $[\text{MgF1}(\text{H}_2\text{O})\text{Cl}]\cdot 2\text{H}_2\text{O}$, $[\text{CaF1}(\text{H}_2\text{O})\text{Cl}]\cdot 3\text{H}_2\text{O}$, $[\text{ZnF1}(\text{H}_2\text{O})\text{Cl}]$, $[\text{FeF1}(\text{H}_2\text{O})_2\text{Cl}_2]\cdot \text{Cl}\cdot 2\text{H}_2\text{O}$, $[\text{MgF2}(\text{H}_2\text{O})\text{Cl}]\cdot 2\text{H}_2\text{O}$, $[\text{CaF2}(\text{H}_2\text{O})\text{Cl}]\cdot 3\text{H}_2\text{O}$, $[\text{ZnF2}(\text{H}_2\text{O})\text{Cl}]$, and $[\text{FeF2}(\text{H}_2\text{O})_2\text{Cl}_2]\cdot \text{Cl}\cdot 2\text{H}_2\text{O}$.

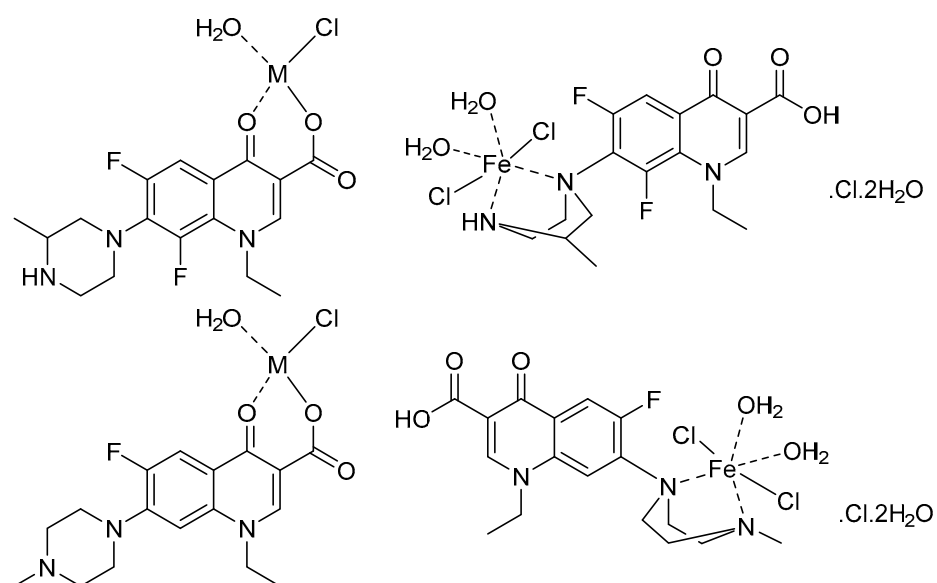


Figure 6. Proposed structures of the F1 and F2 metal-based complexes (M: Mg(II), Ca(II), and Zn(II) ion).

3.4. XRD, SEM, and TEM Results

The XRD diffractograms of the F1 and F2 metal-based complexes are shown in Figure 7. The SEM and TEM micrographs of the F1 and F2 metal-based complexes are presented in Figures 8 and 9, respectively. The XRD diffraction profiles suggested that the Ca(II), Zn(II), and Fe(III) ions tend to form good crystallinity complexes with F1 and F2 with well-defined morphology. The Mg(II) ion forms amorphous complexes with F1 and F2. The strongest diffraction line observed in the XRD patterns for F1 complexes with Mg(II), Ca(II), Zn(II), and Fe(III) was located at Bragg's angle 2θ of 20.212° , 24.008° , 32.668° , and 32.627° , respectively. For F2 complexes, the strongest diffraction line was located at Bragg's angle 2θ of 8.434° , 27.107° , 32.585° , and 32.750° for the Mg(II), Ca(II), Zn(II), and Fe(III) complexes, respectively. Morphologically, the Ca(II)-F1 complex had the most interesting surface topography. Its particles had homogenate short rod-like shaped structures, and these short rods were clustered together to form a tree shape. The Ca(II)-F2 complex rods were longer than the Ca(II)-F1 complex and less homogenate. The Ca(II)-F2 rods do not tend to form a tree shape but accumulated together to form a rough mat. The particles of the Fe(III) complexes with F1 and F2 had a spherical-like morphology. These spherical particles were fused together to form coral reef-like structures. The particles of the Mg(II)-F1 and Mg(II)-F2 complexes tended to form big agglomerates. Complexes of Zn(II) ions with F1 and F2 had cotton-like structures. According to the TEM micrographs, most of the particles of the F1 and F2 complexes exhibited diameters in the range of 30 to 90 nm.

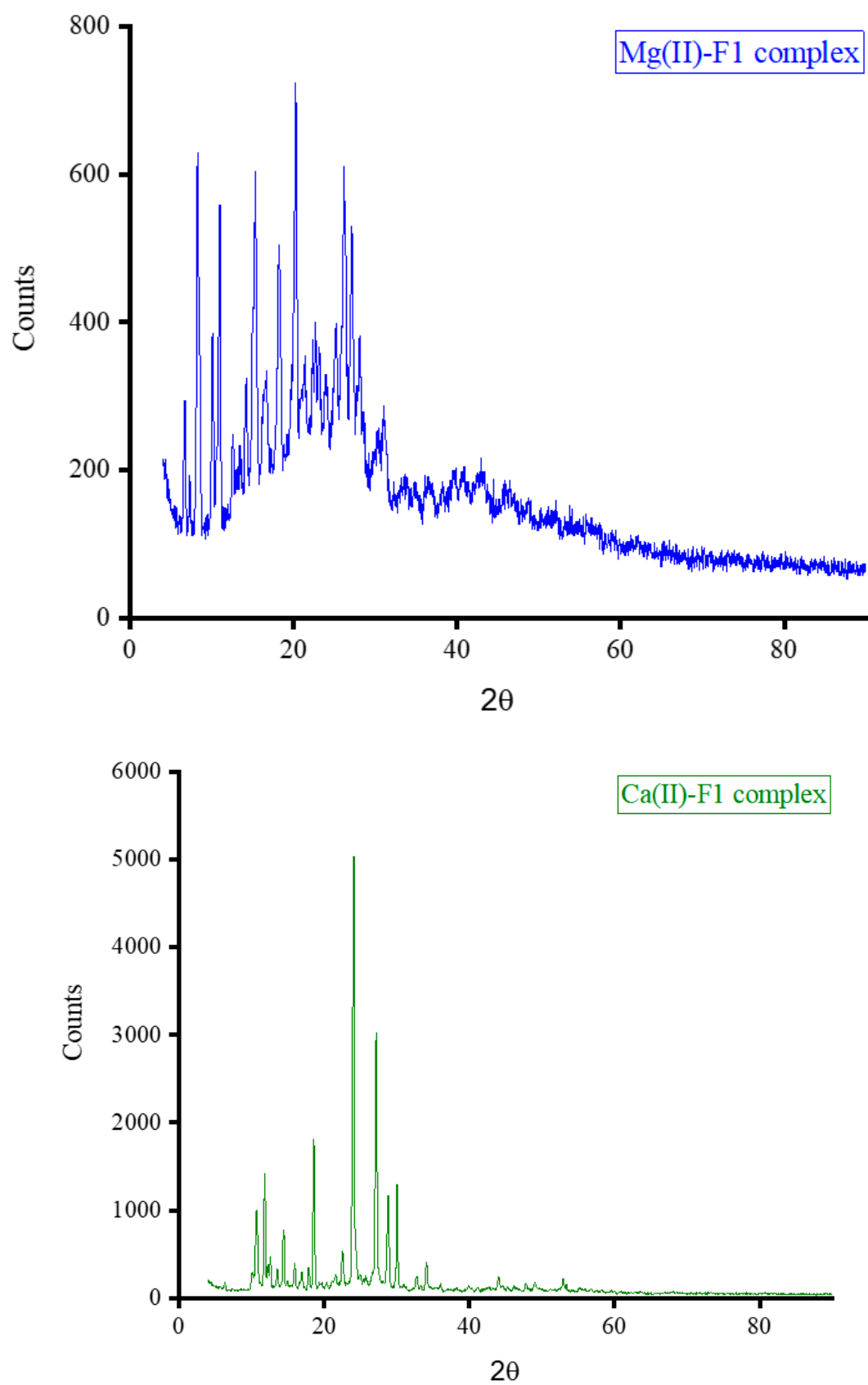


Figure 7. Cont.

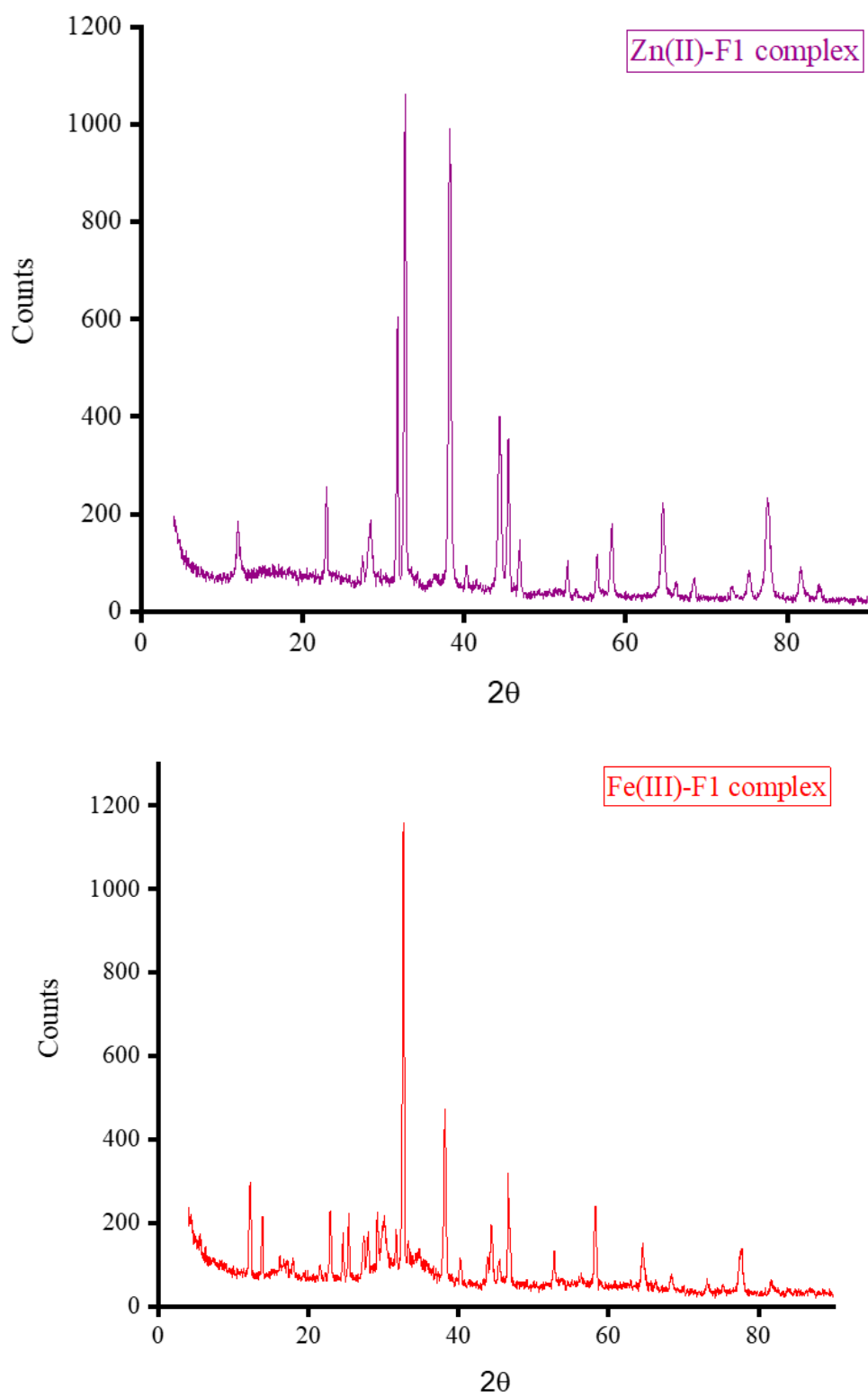


Figure 7. Cont.

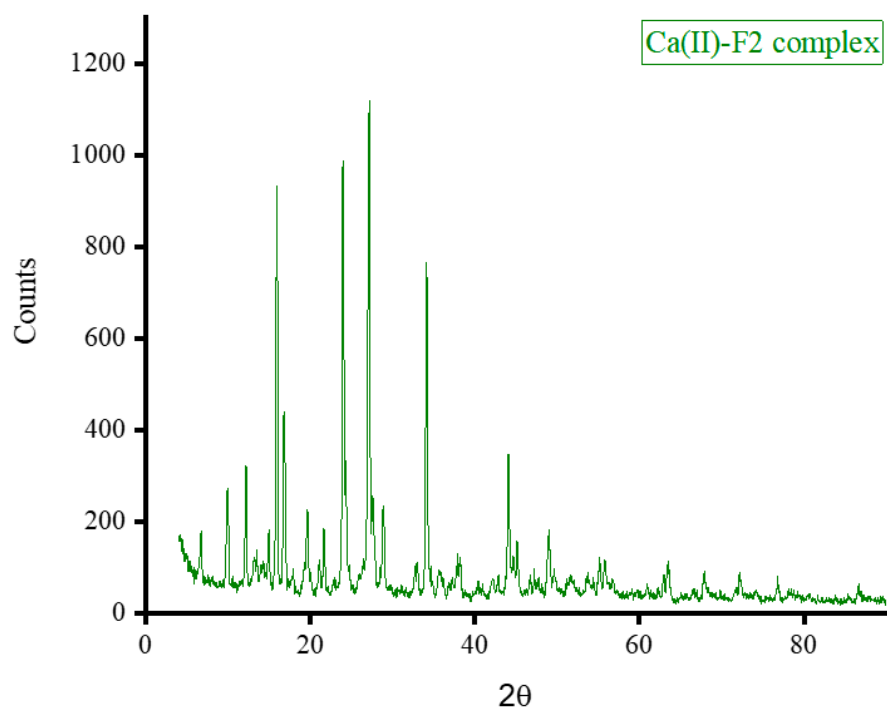
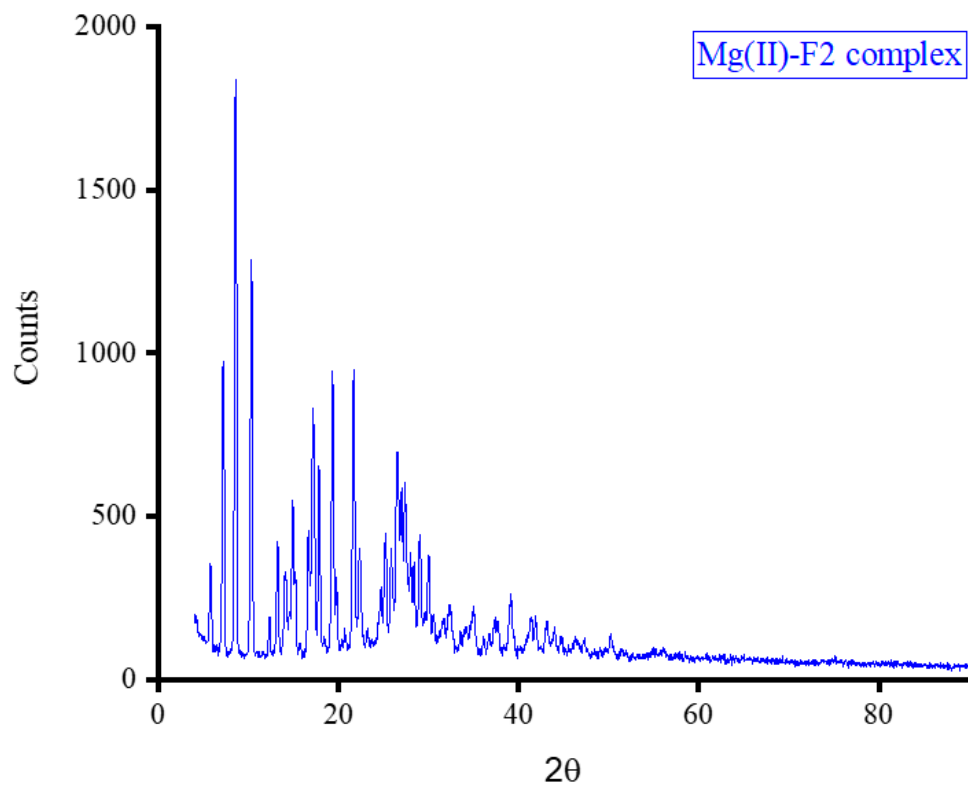


Figure 7. Cont.

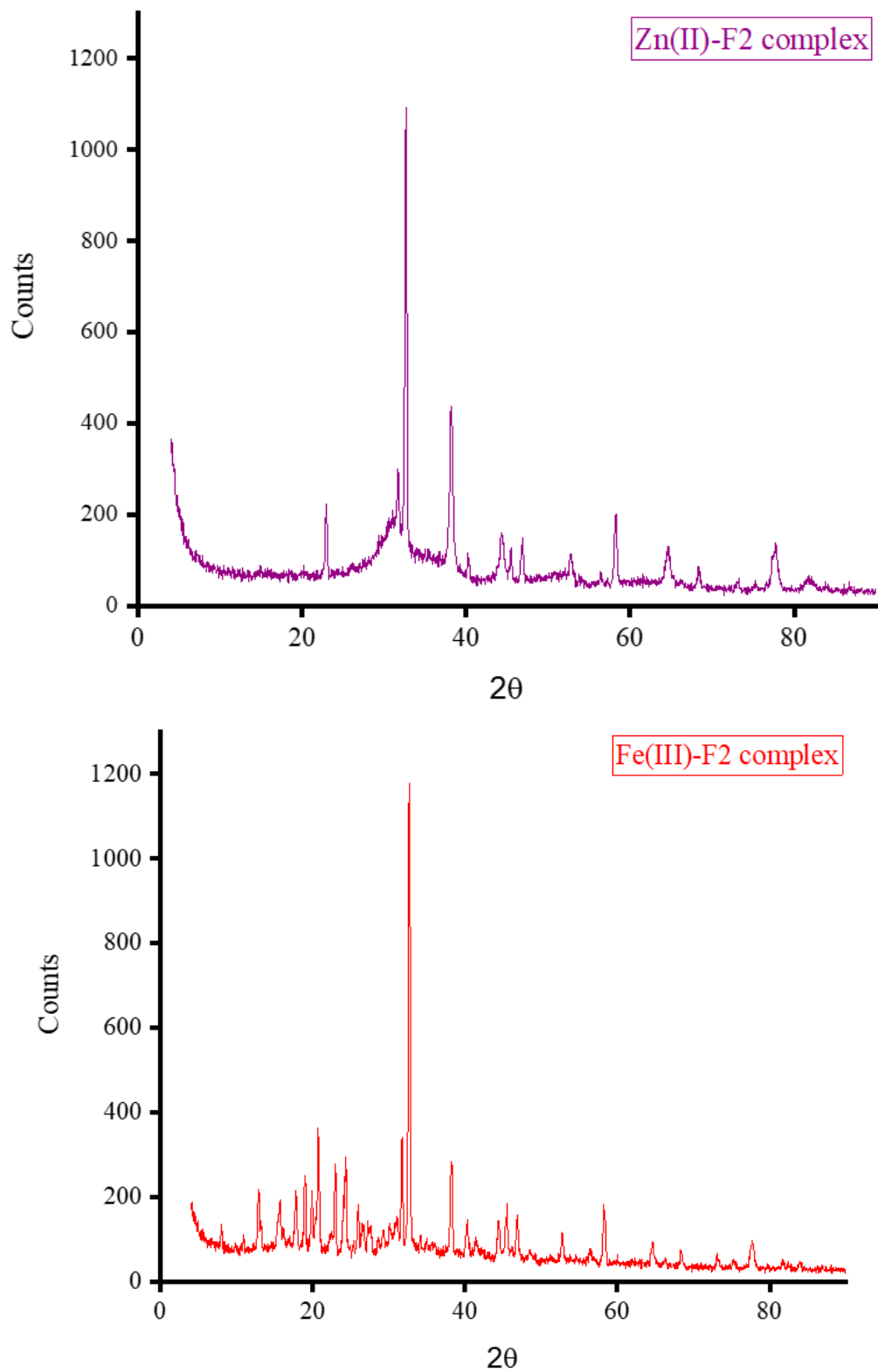


Figure 7. The XRD diffractograms of the F1 and F2 complexes with Mg(II), Ca(II), Zn(II), and Fe(III) ions.

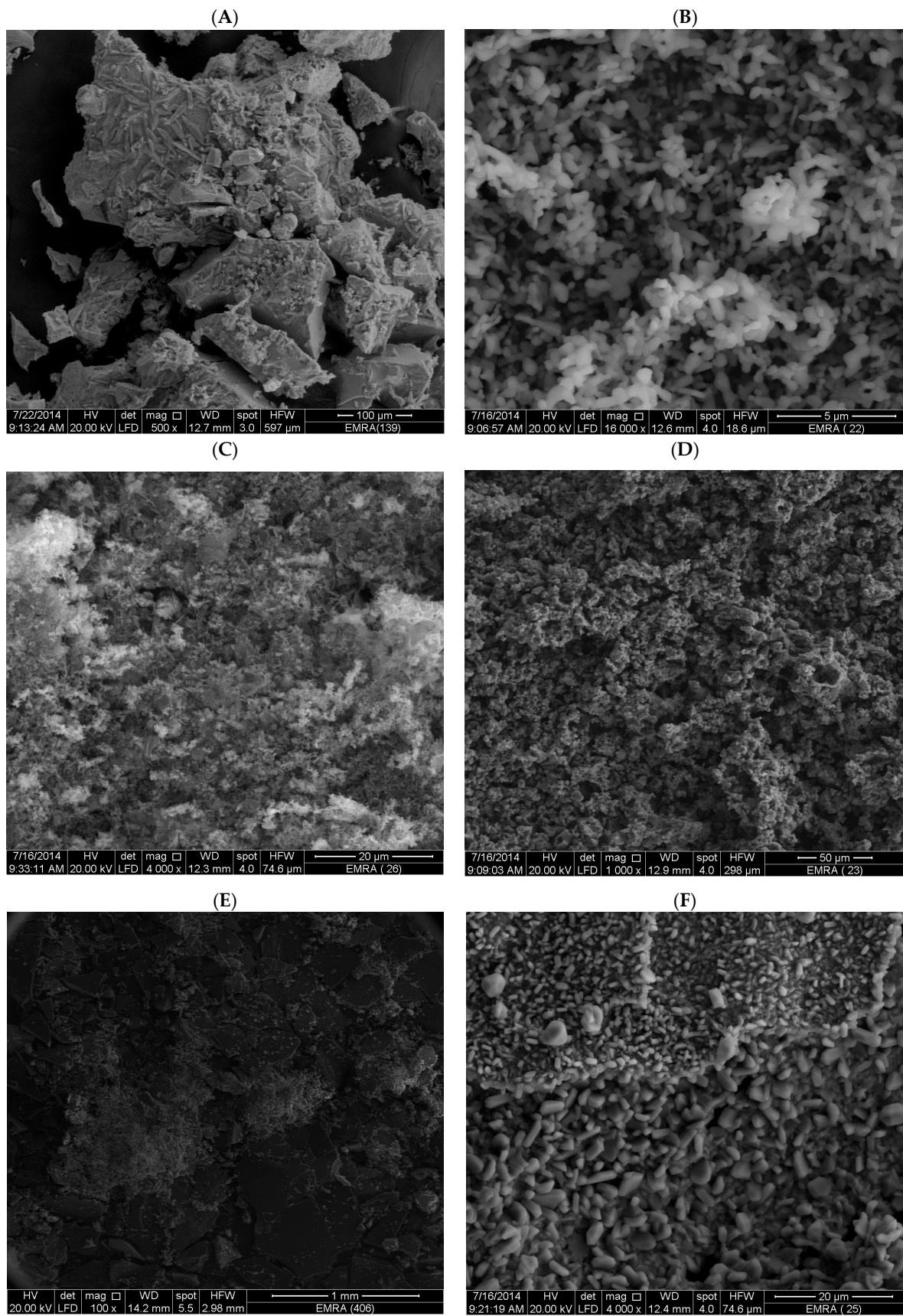


Figure 8. Cont.

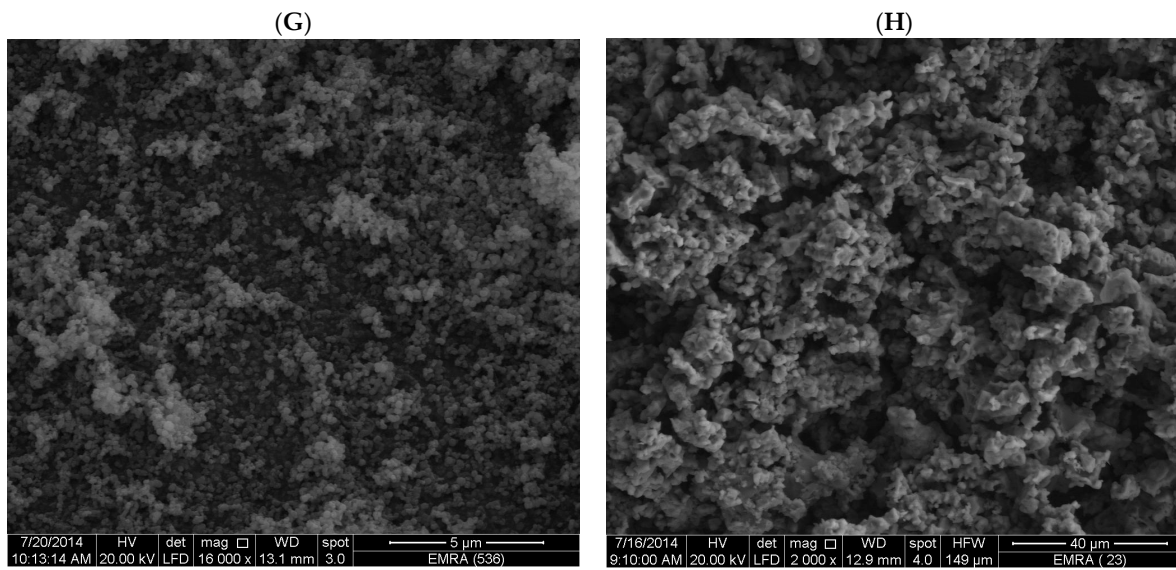


Figure 8. The SEM micrographs of the F1 and F2 complexes: (A) Mg(II)-F1 complex, (B) Ca(II)-F1 complex, (C) Zn(II)-F1 complex, (D) Fe(III)-F1 complex, (E) Mg(II)-F2 complex, (F) Ca(II)-F2 complex, (G) Zn(II)-F2 complex, and (H) Fe(III)-F2 complex.

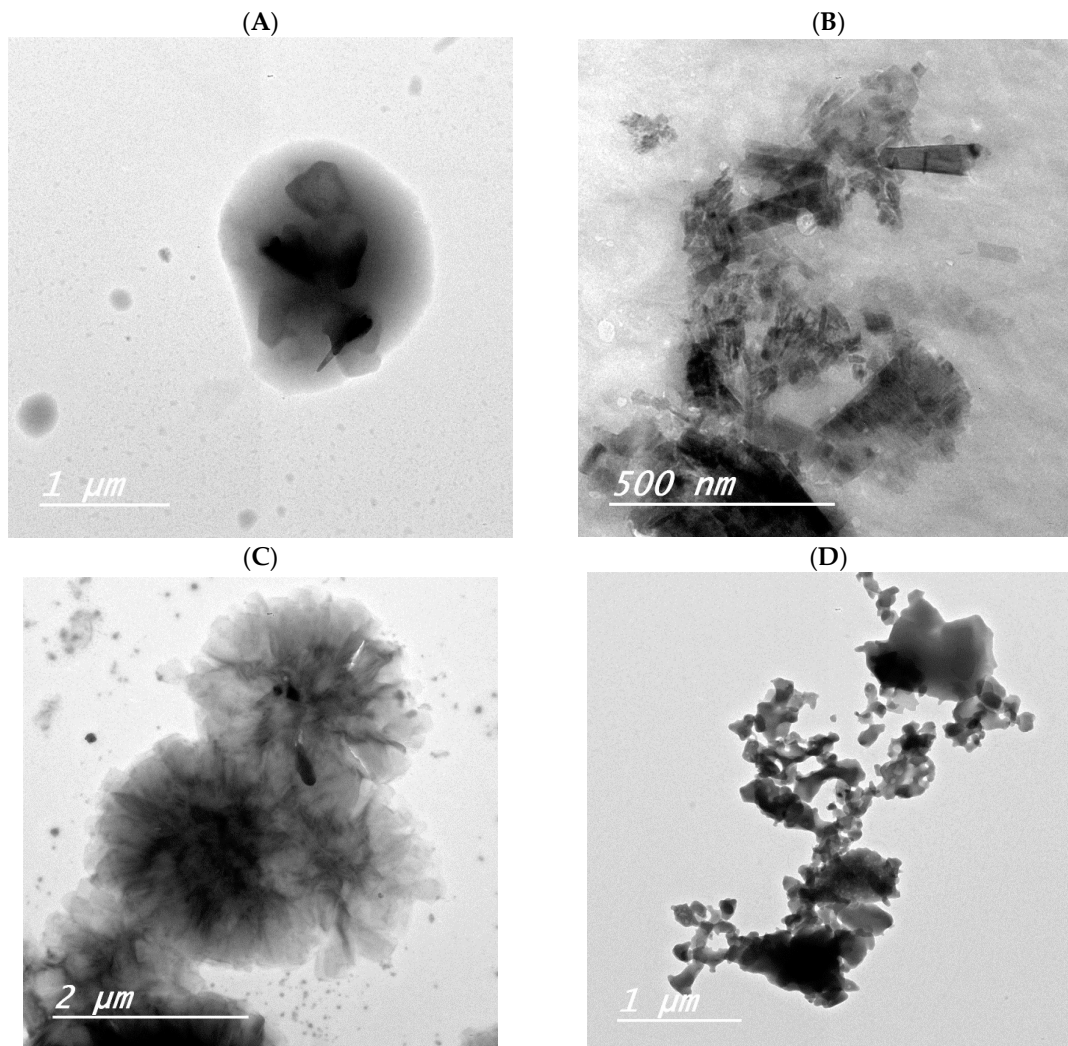


Figure 9. Cont.

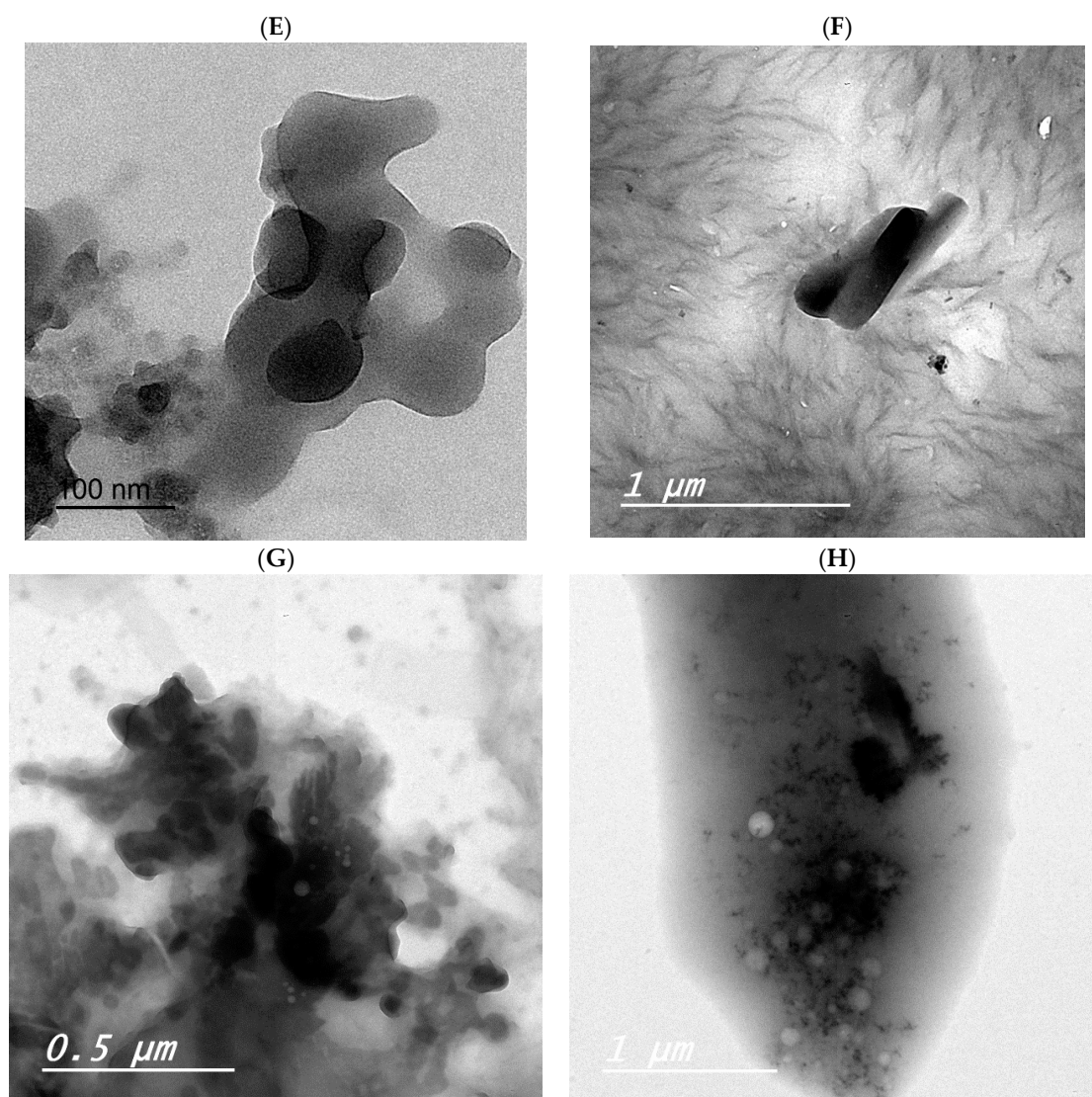


Figure 9. The TEM micrographs of the F1 and F2 complexes: (A) Mg(II)-F1 complex, (B) Ca(II)-F1 complex, (C) Zn(II)-F1 complex, (D) Fe(III)-F1 complex, (E) Mg(II)-F2 complex, (F) Ca(II)-F2 complex, (G) Zn(II)-F2 complex, and (H) Fe(III)-F2 complex.

3.5. Biological Screening

3.5.1. Antibacterial Activity

The well-known Kirby–Bauer disc diffusion protocol assessed the antibacterial properties of the synthesized metal-based complexes in vitro toward three gram-positive bacterial species and two -negative bacterial species. All these bacterial microbes were isolated from clinical samples, and the streptomycin antibiotic drug was used as a positive (+) control for comparison. Table 5 tabulated the zone of inhibition diameter (mm/mg sample) results of the antibacterial potential for the controls ((+); standard drug and (−); DMSO solvent) and the synthesized metal-based complexes.

(a) Screening toward gram-positive bacteria

The inhibition zones (in mm/mg) observed for the standard drug streptomycin were 18.0, 18.0, and 20.0 mm/mg toward *B. subtilis*, *S. pneumoniae*, and *S. aureus*, respectively. Complexes of F1 with Mg(II), Ca(II), and Zn(II) ions showed no or very low activity against the tested gram-positive microbes. The complex of F1 with the Fe(III) ion showed remarkable activity against *S. pneumoniae* and *S. aureus* strains with potency equal to the standard drug streptomycin. Interestingly, when the Fe(III) ion complexed with the

F2 molecule, the resulting complex (Fe(III)-F2) had low activity against the tested gram-positive microbes. The screening results indicated that the complex of F2 with the Mg(II) ion displayed remarkable activity against *B. subtilis* and *S. pneumoniae* species with potency equal to the standard drug streptomycin. Complexes of F2 with Mg(II), Ca(II), and Zn(II) ions were strongly active against the *S. aureus* strain.

(b) Screening toward gram-negative bacteria

The zones of inhibition (in mm/mg) of the standard drug streptomycin toward *E. coli* and *P. aeruginosa* were 22.0 and 27.0 mm/mg, respectively. After it showed remarkable activity toward two species of gram-positive bacteria, the Fe(III)-F1 complex was also strongly active against the tested gram-negative bacterial strains. The rest of the F1 complexes (Mg(II), Ca(II), Zn(II)) had low activity against the tested gram-negative bacteria. This was not the same for the F2 complexes; F2 complexes with Mg(II), Ca(II), and Zn(II) ions had strong potency toward the two tested gram-negative bacteria.

Table 5. Zone of inhibition (mm/mg sample) of the antibacterial activity for the synthesized metal-based complexes.

Sample	Gram-Positive Bacteria Strains			Gram-Negative Bacteria Strains	
	<i>B. subtilis</i>	<i>S. pneumoniae</i>	<i>S. aureus</i>	<i>E. coli</i>	<i>P. aeruginosa</i>
DMSO (–control)	0.0	0.0	0.0	0.0	0.0
Streptomycin (+control)	18.0	17.0	20.0	22.0	27.0
Mg(II)-F1	6.0	1.0	2.0	5.0	4.0
Ca(II)-F1	5.0	3.0	8.0	2.0	8.0
Zn(II)-F1	9.0	5.0	12.0	7.0	3.0
Fe(III)-F1	16.0	19.0	21.0	19.0	24.0
Mg(II)-F2	18.0	20.0	17.0	20.0	18.0
Ca(II)-F2	10.0	15.0	16.0	14.0	19.0
Zn(II)-F2	8.0	11.0	18.0	20.0	24.0
Fe(III)-F2	4.0	13.0	5.0	13.0	14.0

3.5.2. Antifungal Activity

The well-known Kirby–Bauer disc diffusion protocol was also used to assess the antifungal properties of the synthesized metal-based complexes in vitro toward three species: *A. niger*, *Penicillium* sp., and *C. albicans*. Ketoconazole, which was used as positive (+) control, had inhibition values of 18.0, 21.0, and 21.0 mm/mg against the tested fungal species, respectively. Data listed in Table 6 demonstrated that the Fe(III)-F1 complex is the only complex that showed remarkable activity against all tested fungi, with a potency equal to that of the standard drug ketoconazole. Complexes of F1 with Mg(II), Ca(II), and Zn(II) ions had very low-to-low inhibitory activity against the tested fungal species. Complexes of F2 with Mg(II) and Zn(II) ions were strongly active against *Penicillium* sp. and *C. albicans* strains.

In a previous work [31], we investigated the chemical reaction between the quinolone antibiotic oxolinic acid (OA) and Fe(III), Zn(II), Ca(II), and Mg(II) ions. The obtained [Fe(OA)(H₂O)₂Cl₂].2H₂O, [Zn(OA)(H₂O)Cl].2H₂O, [Ca(OA)(H₂O)Cl], and [Mg(OA)(H₂O)Cl] complexes were screened for their antibacterial and antifungal potential. The [Ca(OA)(H₂O)Cl] complex exhibited inhibition against the gram-negative and gram-positive microbes, measuring 27.0, 22.0, 20.0, 17.0, and 18.0 mm/mg for *P. aeruginosa*, *E. coli*, *S. aureus*, *S. pneumoniae*, and *B. subtilis* species, respectively. These results are higher than those observed for the Ca(II)-F1 and Ca(II)-F2 complexes. The Zn(OA)(H₂O)Cl].2H₂O complex exhibited strong antibacterial properties against gram-negative and gram-positive bacteria, except for the

S. pneumoniae strain, with inhibitions of 23.0, 20.0, 18.0, 15.0, and 19.0 mm/mg, respectively. Also, these results are higher than those observed for the Zn(II)-F1 and Zn(II)-F2 complexes. Fe(III)-F1 and Mg(II)-F2 exhibited strong antibacterial properties compared with the $[\text{Fe}(\text{OA})(\text{H}_2\text{O})_2\text{Cl}_2]\cdot 2\text{H}_2\text{O}$ and $[\text{Mg}(\text{OA})(\text{H}_2\text{O})\text{Cl}]\cdot 2\text{H}_2\text{O}$ complexes. The Fe(III)-F1 complex showed remarkable activity against all tested fungi, with a potency equal to the standard drug ketoconazole, while the $[\text{Fe}(\text{OA})(\text{H}_2\text{O})_2\text{Cl}_2]\cdot 2\text{H}_2\text{O}$ complex had no significant effect on the tested fungi, demonstrating only moderate inhibitory activity.

Table 6. Zone of inhibition (mm/mg sample) of the antifungal activity for the synthesized metal-based complexes.

Sample	Fungal Strains		
	<i>A. niger</i>	<i>Penicillium sp.</i>	<i>C. albicans</i>
DMSO (–control)	0.0	0.0	0.0
Ketoconazole (+control)	18.0	21.0	21.0
Mg(II)-F1	2.0	3.0	1.0
Ca(II)-F1	5.0	7.0	1.0
Zn(II)-F1	5.0	9.0	7.0
Fe(II)-F1	19.0	23.0	21.0
Mg(II)-F2	11.0	17.0	18.0
Ca(II)-F2	9.0	11.0	15.0
Zn(II)-F2	15.0	18.0	17.0
Fe(III)-F2	11.0	13.0	12.0

4. Conclusions

The structural and pharmacological properties of Mg(II), Ca(II), Zn(II), and Fe(III) metal ions combined with two fluoroquinolone antibiotics (F1 and F2) were investigated. The metal-based complexes were prepared in neutral media (pH ~7–8) at approximately 60–70 °C using a 1:1 stoichiometric molar ratio and were obtained as white, yellow, and brown powders. The Mg(II), Ca(II), and Zn(II) ions were captured by the oxygen atoms of the carboxylate group and the pyridone C=O group of the F1 and F2 molecules. The F1 and F2 molecules utilized the two nitrogen atoms of the piperazine ring to capture the Fe(III) ion. The Kirby–Bauer disc diffusion assay was employed to determine the in vitro antimicrobial activity of the synthesized metal-based complexes against a broad spectrum of microbes. Among all the metal-based complexes, the Fe(III)-F1 complex exhibited the most potent antimicrobial profile. This complex inhibited the growth of all tested bacterial and fungal species with a potency equal to the standard drugs, streptomycin, and ketoconazole. The next stage of this research will focus on screening the synthesized metal-based complexes (especially those containing Fe(III) ions) for their cytotoxic activity against various human cancer cell lines.

Author Contributions: Conceptualization, R.E. and F.A.A.; methodology, M.A.B. and M.S.R.; software, M.A.B.; validation, R.E., F.A.A. and M.S.R.; formal analysis, F.A.A.; investigation, M.S.R.; resources, M.A.B.; data curation, R.E.; writing—original draft preparation, A.M.A.A.; writing—review and editing, A.M.A.A.; visualization, A.M.N.; supervision, A.A.A., M.A.A.-O. and A.M.N.; project administration, A.A.A., M.A.A.-O. and A.M.N.; funding acquisition, A.A.A., M.A.A.-O. and A.M.N. All authors have read and agreed to the published version of the manuscript.

Funding: This research was funded by the Deputyship for Research and Innovation, Ministry of Education in Saudi Arabia, through project No. (IFKSURC-1-0127).

Data Availability Statement: The data presented in this study are available on request from the corresponding author.

Acknowledgments: The authors extend their appreciation to the Deputyship for Research and Innovation, Ministry of Education in Saudi Arabia, for funding this research. (IFKSURC-1-0127.)

Conflicts of Interest: The authors declare no conflict of interest.

References

1. Tella, A.C.; Obaleye, J.A.; Olawale, M.D.; Ngororabanga, J.M.V.; Ogunlaja, A.S.; Bourned, S.A. Synthesis, crystal structure, and density functional theory study of a zinc(II) complex containing terpyridine and pyridine-2,6-dicarboxylic acid ligands: Analysis of the interactions with amoxicillin. *Comptes Rendus Chimie* **2019**, *22*, 3–12. [[CrossRef](#)]
2. Eichhorn, G.L.; Marzilli, L.G. *Advances in Inorganic Biochemistry Models in Inorganic Chemistry*; PTR Prentice-Hall, Inc.: Englewood Cliffs, NJ, USA, 1994.
3. Hughes, M.N. *The Inorganic Chemistry of Biological Processes*, 2nd ed.; Wiley: Chichester, UK, 1984.
4. Alessio, E. *Bioinorganic Medicinal Chemistry*; Wiley-VCH Verlag GmbH and Co. KGaA: Weinheim, Germany, 2011.
5. FTrudu; Amato, F.; Vaňhara, P.; Pivetta, T.; Peña-Méndez, E.M.; Havel, J. Coordination compounds in cancer: Past, present and perspectives. *J. Appl. Biomed.* **2015**, *13*, 79.
6. Singh, U.; Malla, A.M.; Bhat, I.A.; Ahmad, A.; Bukhari, M.N.; Bhat, S.; Anayutullah, S.; Hashmi, A.A. Synthesis, molecular docking and evaluation of antifungal activity of Ni(II),Co(II) and Cu(II) complexes of porphyrin core macromolecular ligand. *Microb. Pathog.* **2016**, *93*, 172. [[CrossRef](#)] [[PubMed](#)]
7. Netalkar, P.P.; Netalkar, S.P.; Revankar, V.K. Transition metal complexes of thiosemicarbazone: Synthesis, structures and invitro antimicrobial studies. *Polyhedron* **2015**, *100*, 215. [[CrossRef](#)]
8. Ragheb, M.A.; Eldesouki, M.A.; Mohamed, M.S. DNA binding, photo-induced DNA cleavage and cytotoxicity studies of lomefloxacin and its transition metal complexes. *Spectrochim. Acta A* **2015**, *138*, 585. [[CrossRef](#)]
9. Sana, S.S.; Hou, T.; Li, H.; Vadde, R.; Basavegowda, N.; Chakravorty, A.; Kumbhakar, D.V.; Zhang, Z.; Mamidi, N. Crude Polysaccharide Produces Silver Nanoparticles with Inherent Antioxidant and Antibacterial Activity. *ChemistrySelect* **2023**, *8*, e202203658. [[CrossRef](#)]
10. Tabassum, Z.; Mohan, A.; Mamidi, N.; Khosla, A.; Kumar, A.; Solanki, P.R.; Malik, T.; Girdhar, M. Recent trends in nanocomposite packaging films utilising waste generated biopolymers: Industrial symbiosis and its implication in sustainability. *IET Nanobiotechnol.* **2023**, *17*, 127–153. [[CrossRef](#)]
11. Sana, S.S.; Vadde, R.; Kumar, R.; Arla, S.K.; Somala, A.R.; Rao, K.K.; Zhijun, Z.; Boya, V.K.N.; Mondal, K.; Mamidi, N. Eco-friendly and facile production of antibacterial zinc oxide nanoparticles from *Grewia flavescens* (*G. flavescens*) leaf extract for biomedical applications. *J. Drug Deliv. Sci. Technol.* **2023**, *80*, 104186. [[CrossRef](#)]
12. Fricker, S.P. Metal based drugs: From serendipity to design. *Dalton Trans.* **2007**, *43*, 4903. [[CrossRef](#)]
13. Jurowska, A.; Jurowski, K.; Szklarzewicz, J.; Buszewski, B.; Kalenik, T.; Piekoszewski, W. Molybdenum Metallopharmaceuticals Candidate Compounds - The “Renaissance” of Molybdenum Metallodrugs? *Cur. Med. Chem.* **2016**, *23*, 3322. [[CrossRef](#)]
14. Efthimiadou, E.K.; Thomadaki, H.; Sanakis, Y.; Raptopoulou, C.P.; Katsaros, N.; Scorilas, A.; Karaliota, A.; Psomas, G. Structure and biological properties of the copper(II) complex with the quinolone antibacterial drug *N*-propyl-norfloxacin and 2,2'-bipyridine. *J. Inorg. Biochem.* **2007**, *101*, 64. [[CrossRef](#)] [[PubMed](#)]
15. Vieira, L.M.M.; de Almeida, M.V.; Lourenço, M.C.S.; Bezerra, F.A.F.M.; Fontes, A.P.S. Synthesis and antitubercular activity of palladium and platinum complexes with fluoroquinolones. *Eur. J. Med. Chem.* **2009**, *44*, 4107–4111. [[CrossRef](#)] [[PubMed](#)]
16. Sadeek, S.A.; El-Shwiniy, W.H. Preparation, structure and microbial evaluation of metal complexes of the second generation quinolone antibacterial drug lomefloxacin. *J. Mol. Struct.* **2010**, *98*, 130. [[CrossRef](#)]
17. El-Halim, H.F.A.; Mohamed, G.G.; El-Dessouky, M.M.I.; Mahmoud, W.H. Ligational behaviour of lomefloxacin drug towards Cr(III), Mn(II), Fe(III), Co(II), Ni(II), Cu(II), Zn(II), Th(IV) and UO₂(VI) ions: Synthesis, structural characterization and biological activity studies. *Spectrochim. Acta A* **2011**, *82*, 8. [[CrossRef](#)]
18. Qi, W.; Huang, J.; An, Z. Aqua-bis[1-ethyl-6-fluoro-7-(4-methyl-piperazin-1-yl)-4-oxo-1,4-dihydro-quinoline-3-carboxylato]zinc(II) dihydrate. *Acta Crystallogr.* **2008**, *64*, m302.
19. Drevenšek, P.; Košmrlj, J.; Giester, G.; Skauge, T.; Sletten, E.; Sepčić, K.; Turel, I. X-Ray crystallographic, NMR and antimicrobial activity studies of magnesium complexes of fluoroquinolones – racemic ofloxacin and its *S*-form, levofloxacin. *J. Inorg. Biochem.* **2006**, *100*, 1755. [[CrossRef](#)]
20. Bauer, A.W.; Kirby, W.M.M.; Sherris, J.C.; Turck, M. Antibiotic susceptibility testing by a standardized single disk method. *Am. J. Clin. Pathol.* **1966**, *45*, 493–496. [[CrossRef](#)]
21. Biemer, J.J. Antimicrobial susceptibility testing by the Kirby-Bauer disc diffusion method. *Ann. Clin. Lab. Sci.* **1973**, *3*, 135–140.
22. MSerrano, C.; Ramírez, M.; Morilla, D.; Valverde, A.; Chávez, M.; Espinel-Ingroff, A.; Claro, R.; Fernández, A.; Almeida, C.; Martín-Mazuelos, E. A comparative study of the disc diffusion method with the broth microdilution and Etest methods for voriconazole susceptibility testing of *Aspergillus* spp. *J. Antimicrob. Chemother.* **2004**, *53*, 739–742. [[CrossRef](#)]
23. Allan, J.R.; Baird, N.D.; Kassyk, A.L. Some first row transition metal complexes of nicotinamide and nicotinic acid. *J. Therm. Anal. Calorim.* **1979**, *16*, 79–90. [[CrossRef](#)]
24. Öztirk, F.; Şekerci, M.; Özdemir, E. Preparation of complexes of 1-amino-6,7-O-cyclohexylidene-4-azaheptane with transition metal acetates. *Russ. J. Gen. Chem.* **2006**, *76*, 33–36. [[CrossRef](#)]
25. Refat, M.S.; El-Sayed, M.Y.; Hassan, R.F. Study of the chemical structure and the microbial effect of iron(III) metal ions with four consecutive generations of quinolones in a nanometric form for the purpose of increasing the efficacy of antibacterial and antifungal drugs. *Appl. Organomet. Chem.* **2017**, *32*, e4195. [[CrossRef](#)]
26. Deacon, G.B.; Phillips, R. Relationships between the carbon-oxygen stretching frequencies of carboxylato complexes and the type of carboxylate coordination. *Coord. Chem. Rev.* **1980**, *33*, 227–250. [[CrossRef](#)]

27. Nakamoto, K. *Infrared Spectra of Inorganic and Coordination Compounds*, 2nd ed.; Wiley Interscience, John Wiley & Sons: New York, NY, USA, 1970.
28. El-Megharbel, S.M.; Hegab, M.S.; Manaaa, E.-S.A.; Al-Humaidi, J.Y.; Refat, M.S. Synthesis and physicochemical characterizations of coordination between palladium(ii) metal ions with floroquinolone drugs as medicinal model against cancer cells: Novel metallopharmaceuticals. *New J. Chem.* **2018**, *42*, 9709–9719. [[CrossRef](#)]
29. El-Megharbel, S.M.; A Hussien, M.; Refat, M.S. In-Situ Copper(II) Complexes of Some Quinolone Drug Ligands Were Discussed for Their Molecular Structures: Synthesis in Binary Solvent. *J. Comput. Theor. Nanosci.* **2017**, *14*, 561–576. [[CrossRef](#)]
30. Nassar, M.W.; Attia, K.A.M.; Said, R.A.; El-Olemy, A.; Hasan, M.A. Second Derivative Synchronous Spectrofluorimetric Determination of Lomefloxacin Hydrochloride in Presence of Its Decarboxylated Degradation Product. *Ijppr. Hum.* **2017**, *11*, 397–418.
31. Almehizia, A.A.; Al-Omar, M.A.; Naglah, A.M.; Bhat, M.A.; Alanazi, F.S.; Alotaibi, F.A.; Refat, M.S.; Adam, A.M.A. Complexes of the Antibiotic Drug Oxolinic Acid with Fe(III), Zn(II), Ca(II), and Mg(II) Ions: Preparation, Characterization, and In Vitro Evaluation of Biological Activity. *Crystals* **2023**, *13*, 1012. [[CrossRef](#)]

Disclaimer/Publisher's Note: The statements, opinions and data contained in all publications are solely those of the individual author(s) and contributor(s) and not of MDPI and/or the editor(s). MDPI and/or the editor(s) disclaim responsibility for any injury to people or property resulting from any ideas, methods, instructions or products referred to in the content.